

A Grad-Shafranov model for compact quasisymmetric stellarators

N. Nikulsin,¹ W. Sengupta,¹ S. Buller,¹ and A. Bhattacharjee¹

Department of Astrophysical Sciences, Princeton University, Princeton, NJ 08544, USA

(*Electronic mail: nnikulsin@princeton.edu)

(Dated: 22 January 2025)

A Grad-Shafranov equation (GSE) valid for compact quasisymmetric stellarators is derived by an asymptotic expansion around a vacuum field carried to first order. We obtain an equation for the existence of flux surfaces leading up to the GSE. The flux surface label must simultaneously satisfy the existence equation and the GSE, which generally leads to an overdetermined problem. We show how the overdetermined problem can be resolved within our model for a class of hybrid devices similar to that studied by Henneberg and Plunk (S. Henneberg and G. Plunk, PRR 2024). We are also able to solve the existence equation for flux surfaces analytically in the most general case by introducing a special coordinate system. In future work, we plan to carry out an optimization seeking to minimize the error in our GSE while obeying the flux surface existence equation. This should be faster than a conventional stellarator optimization and will allow us to find solutions outside the class of hybrid devices.

I. INTRODUCTION

Compact magnetic fusion devices have attracted some interest due to their potential to significantly reduce the cost of a future fusion power plant¹. While most studies of compact devices have focused on spherical tokamaks^{2–4}, compact stellarators of the quasi-axisymmetric (QA) type, such as NCSX have also been considered⁵. Recently, a QA device that is a hybrid of a tokamak and stellarator has been proposed⁶. Such a device would be axisymmetric on the outboard side but have helical corrugations, which would provide a source of external rotational transform on the inboard side. These corrugations are produced by a set of "banana coils," which are also located on the inboard side. Aside from the banana coils, the only other type of coils that are necessary are tokamak-like planar toroidal field coils. Thus, the complexity of coils necessary for constructing such a device is greatly reduced compared to contemporary modular coil stellarators.

It should be noted that the concept of a compact stellarator with helical corrugations on the inboard side and an axisymmetric outboard side has been considered by Moroz already in 1998⁷, long before Ref 6. However, the novelty of Ref 6 was in showing that such a stellarator can be optimized for quasi-axisymmetry. Quasisymmetry, of which quasi-axisymmetry is a special case, is one of two main approaches to confining particle orbits inside a stellarator^{8,9}. The simplest way to define quasisymmetry is as a stellarator configuration where the magnetic field satisfies $|\vec{B}| = B(\psi, M\theta - N\phi)$, where M, N are arbitrary integers and (ψ, θ, ϕ) is a straight field line coordinate system⁸. The case when $N = 0$ corresponds to quasi-axisymmetry. Thus, a quasisymmetric magnetic field has a magnitude that depends only on two coordinates, but the full magnetic field vector can still depend on all three coordinates.

A significant complication that arises when designing quasisymmetric stellarators is that the MHD equilibrium equations (with isotropic pressure) already comprise a closed system of equations, and imposing the quasisymmetry condition on $|\vec{B}|$ appears to overdetermine the system, requiring a careful optimization procedure to find a satisfactory configuration¹⁰. Within the context of the near-axis expansion^{11–14}, which consists of Taylor-expanding all quan-

ties of interest in the radial coordinate and balancing the coefficients of the MHD equilibrium equations at each order of the expansion, resulting in a system of ordinary differential and algebraic equations, the overconstraining problem is absent at first order¹¹. At second order, the problem can be dealt with by not imposing quasisymmetry directly, but instead optimizing for it, which is much faster than traditional optimization due to the smaller parameter space¹⁵. At third order and beyond, the system of equations is severely overdetermined, and there is evidence that the Taylor series itself begins to diverge¹⁶.

The near-axis model, however, cannot be applied to low aspect ratio devices like the Henneberg-Plunk stellarator described in Ref 6. In this paper, we will apply a Grad-Shafranov model¹⁷ simpler versions of which were considered in Refs 18 and 19, to study a Henneberg-Plunk-like device. In previous papers^{18,19}, the model was derived via an expansion in the inverse aspect ratio. However, a more general expansion in the deviation of the total magnetic field from the coil-generated field is also possible. Indeed, in Ref 19, we show that, under the assumptions made in that paper, such an expansion is equivalent to a large-aspect-ratio expansion. It should be noted that a GSE for quasisymmetric stellarators was derived without any expansions or approximations in Ref 20. However, that paper does not address the overdetermination problem or attempt to solve the equation. In this paper, we will consider the overdetermination problem head-on and propose an approach to resolving it for a particular kind of compact quasisymmetric device.

The rest of this paper is organized as follows. In section II, we will derive the model under a slightly different set of assumptions than in Ref 19, which allow for compact geometries. Then, in section III, we will apply the newly derived model to a Henneberg-Plunk-like stellarator to demonstrate its utility. The approximate solution obtained in section III will then be refined via conventional stellarator optimization in section IV. Finally, we conclude in section V by discussing further work that could allow this model to be applied to a broader class of compact stellarators.

II. DERIVATION

In Ref 19, we expanded the magnetic field around a vacuum magnetic field $\nabla\chi$ (χ is the magnetic scalar potential):

$$\vec{B} = \left(1 + \frac{B_1}{B_v}\right) \nabla\chi + \nabla A \times \nabla\chi + O(\varepsilon^2), \quad (1)$$

under the assumption that $B_v = |\nabla\chi| = O(1)$, $B_1 = O(\varepsilon)$, where $\varepsilon = \max|\vec{B} - \nabla\chi|/B_v \ll 1$ and $A = O(\varepsilon)$ is a stream function needed to represent perturbations perpendicular to $\nabla\chi$. As is usually the case in reduced MHD models, we also order the derivative along the vacuum field as $\nabla\chi \cdot \nabla = O(\varepsilon)$, whereas $\nabla_\perp = \nabla - B_v^{-1} \nabla\chi \cdot \nabla = O(1)$. As discussed in Ref 19, this last ordering can be justified by considering the length scales in each direction.

The current density can be written in two different ways, one of which is obtained from the definition of the current density and the other from the MHD equilibrium equation:

$$\vec{j} = \frac{\vec{B} \times \nabla p}{B^2} + j_\parallel \frac{\vec{B}}{B} = \frac{\nabla\chi \times \nabla p}{B_v^2} - \frac{\vec{B}}{\mu_0} \Delta^* A + O(\varepsilon^2), \quad (2a)$$

$$\vec{j} = \frac{1}{\mu_0} \nabla \times \vec{B} = \frac{1}{\mu_0} \nabla \left(\frac{B_1}{B_v} \right) \times \nabla\chi - \frac{\nabla\chi}{\mu_0} \nabla^2 A + O(\varepsilon^2), \quad (2b)$$

where $\Delta^* = B_v^{-2} \nabla \cdot (B_v^2 \nabla_\perp)$.

As we showed in Ref 19, in order for the perpendicular components of both equations (2) to match, either the aspect ratio must be large, or we must have $B_1 = 0$ and $p = O(\varepsilon^2)$. We have already considered the first case in Ref 19; we will now study the second case, which allows for compact geometries. Thus, expression (1) becomes

$$\vec{B} = \nabla\chi + \nabla A \times \nabla\chi, \quad (3)$$

which we will use throughout the rest of this paper.

A. Obtaining the pre-Grad-Shafranov equation

Taking the divergence of equation (2a), we obtain the main equation, which can be transformed to a Grad-Shafranov equation in the case of quasisymmetric stellarators:

$$\begin{aligned} \vec{B} \cdot \nabla \left(\frac{j_\parallel}{B} \right) + \nabla \cdot \left(\frac{\vec{B} \times \nabla p}{B^2} \right) \\ = \frac{-1}{\mu_0} \vec{B} \cdot \nabla \Delta^* A + \nabla \cdot \left(\frac{1}{B_v^2} \right) \cdot (\nabla\chi \times \nabla p) + O(\varepsilon^3) = 0. \end{aligned} \quad (4)$$

To close the system, we also need an equation for p , which is simply $\vec{B} \cdot \nabla p = 0$.

We can now impose the two-term quasisymmetry condition, which is equivalent to demanding that $|\vec{B}| = B(\psi, M\theta - N\phi)$: $(\vec{B} \times \nabla\psi) \cdot \nabla B = F(\psi) \vec{B} \cdot \nabla B$, where ψ is the toroidal flux⁸. Under our ordering, this condition can be written in two equivalent ways:

$$(\nabla\chi \times \nabla\Psi) \cdot \nabla B_v = \vec{B} \cdot \nabla B_v, \quad (5a)$$

$$(\nabla B_v \times \nabla\chi) \cdot \nabla(\Psi + A) = \nabla\chi \cdot \nabla B_v, \quad (5b)$$

where $\Psi = \int d\psi/F(\psi)$ is defined to absorb the $F(\psi)$ factor. Note that⁸ $F(\psi)$ is $O(\varepsilon^{-1})$, so $\Psi = O(\varepsilon)$. Using (5a), the second term in the RHS of equation (4) can be rewritten as $(dp/d\Psi)(\nabla\chi \times \nabla\Psi) \cdot \nabla B_v^{-2} = (dp/d\Psi) \vec{B} \cdot \nabla B_v^{-2}$, which results in both terms in the equation having $\vec{B} \cdot \nabla$ acting on something. We then remove the $\vec{B} \cdot \nabla$ operator, obtaining a Grad-Shafranov-like equation:

$$\Delta^* A - \frac{\mu_0}{B_v^2} \frac{dp}{d\Psi} = H(\Psi). \quad (6)$$

B. A coordinate system for near-vacuum quasisymmetry

We introduce a new coordinate system, (B_v, s, χ) , where B_v and χ are as defined above and s is an arbitrary third coordinate. One can choose s to be any quantity as long as the Jacobian is nonsingular in the region of interest. Using these coordinates, we can rewrite equation (5b) as

$$\frac{1}{\sqrt{g}} \frac{\partial}{\partial s} (\Psi + A) = g^{B_v \chi},$$

where g is the metric tensor. Integrating over s , we obtain an algebraic relation between A and Ψ :

$$\begin{aligned} \Psi + A = -I + a(B_v, \chi), \\ I = \int g^{B_v \chi} \sqrt{g} ds = \int \frac{\nabla\chi \cdot \nabla B_v}{(\nabla B_v \times \nabla s) \cdot \nabla\chi} ds, \end{aligned} \quad (7)$$

where $a(B_v, \chi)$ is an arbitrary function that appears due to the integration.

Now consider the equation $\vec{B} \cdot \nabla p = 0$. Since $p = p(\Psi)$, using equations (3) and (7), we have

$$\vec{B} \cdot \nabla \Psi = B_v^2 \frac{\partial \Psi}{\partial \chi} + g^{s\chi} \frac{\partial \Psi}{\partial s} + \frac{1}{\sqrt{g}} \frac{\partial \Psi}{\partial s} \left(\frac{\partial I}{\partial B_v} - \frac{\partial a}{\partial B_v} \right) = 0. \quad (8)$$

This equation can be further simplified by considering the fact that χ must satisfy the Laplace equation. Using the expression for divergence in general non-orthogonal coordinates, one has

$$\begin{aligned} \sqrt{g} \nabla^2 \chi &= \frac{\partial}{\partial q^k} \left[\sqrt{g} (\nabla\chi)^k \right] \\ &= \frac{\partial}{\partial B_v} (g^{B_v \chi} \sqrt{g}) + \frac{\partial}{\partial s} (g^{s\chi} \sqrt{g}) + B_v^2 \frac{\partial}{\partial \chi} \sqrt{g} = 0. \end{aligned}$$

Integrating this equation over s , we obtain

$$\frac{\partial I}{\partial B_v} = -g^{s\chi} \sqrt{g} - B_v^2 \frac{\partial}{\partial \chi} \int \sqrt{g} ds + \tilde{a}(B_v, \chi). \quad (9)$$

Substituting this into equation (8) yields:

$$B_v^2 \frac{\partial \Psi}{\partial \chi} - \frac{1}{\sqrt{g}} \frac{\partial \Psi}{\partial s} \left(B_v^2 \frac{\partial}{\partial \chi} \int \sqrt{g} ds + \frac{\partial a}{\partial B_v} \right) = 0, \quad (10)$$

where \tilde{a} has been absorbed into $\partial a/\partial B_v$. The Lagrange-Charpit equation is then

$$\begin{aligned} \frac{ds}{d\chi} &= \frac{-1}{B_v^2 \sqrt{g}} \left(B_v^2 \frac{\partial}{\partial \chi} \int \sqrt{g} ds + \frac{\partial a}{\partial B_v} \right) \\ &= - \left(\frac{\partial U}{\partial s} \right)^{-1} \frac{\partial U}{\partial \chi} - \frac{1}{B_v^2} \left(\frac{\partial U}{\partial s} \right)^{-1} \frac{\partial a}{\partial B_v}, \end{aligned}$$

where $U = \int \sqrt{g} ds$. Thus, the characteristics are

$$\begin{aligned} C_1 &= B_v, \\ C_2 &= U + \frac{1}{B_v^2} \int \frac{\partial a}{\partial B_v} d\chi = \int \sqrt{g} ds + \frac{1}{B_v^2} \int \frac{\partial a}{\partial B_v} d\chi, \end{aligned} \quad (11)$$

and the solution of equation (10) is $\Psi = \Psi(C_1, C_2)$.

C. The final Grad-Shafranov equation

To obtain the Grad-Shafranov equation, we insert relation (7) into the pre-Grad-Shafranov equation (6), yielding

$$\Delta^* \Psi + \Delta^*(I - a) = -\frac{\mu_0}{B_v^2} \frac{dp}{d\Psi} - H(\Psi). \quad (12)$$

Note that Ψ is overconstrained: it must simultaneously satisfy both equations (12) and (10). Formulated another way, Ψ must be a function of only C_1 and C_2 , while the terms on the LHS of equation (12) can, in general, be functions of all three variables. In the next section, we will consider a special case where the overconstraining problem is resolved. Solving the problem in general would require implementing a numerical solver that constructs a function basis in C_1, C_2 space and then looking for functions that minimize the error in equation (12). We will return to this task in future work.

Finally, we note that the Δ^* operator can be written in the (B_v, s, χ) coordinates as

$$\begin{aligned} \Delta^* &= \frac{g^{B_v B_v}}{B_v^2} \frac{\partial}{\partial B_v} \left(B_v^2 \frac{\partial}{\partial B_v} \right) + \frac{2g^{B_v s}}{B_v} \frac{\partial}{\partial B_v} \left(B_v \frac{\partial}{\partial s} \right) \\ &+ g^{ss} \frac{\partial^2}{\partial s^2} + \Delta B_v \frac{\partial}{\partial B_v} + \Delta s \frac{\partial}{\partial s} + O(\varepsilon). \end{aligned} \quad (13)$$

III. A HYBRID HENNEBERG-PLUNK-LIKE COMPACT QAS: AN APPLICATION

To illustrate the use of the model derived in the previous section, we will consider a device similar to the compact quasisymmetric stellarator configuration presented in Ref 6. We do not attempt to model the exact device presented in Ref 6 but rather study a similar device based on the same design principles, namely, an axisymmetric outboard side and helical corrugations on the inboard side.

As was discussed in the previous section, one of the main difficulties with quasisymmetry is that the corresponding system of equations is overconstrained. However, as is known

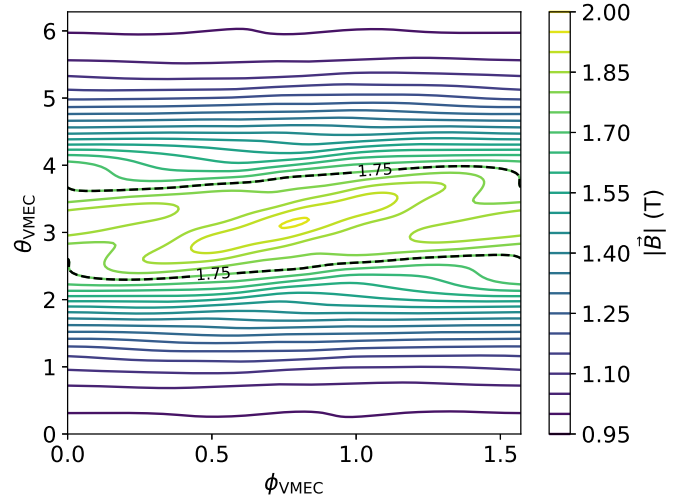


FIG. 1. The magnetic field strength on the outermost flux surface of the Henneberg-Plunk stellarator⁶. The field strength in between the two dashed lines ranges from 1.75 T to 2 T.

from the tokamak theory, this overconstraining problem is trivially resolved in the axisymmetric case. Thus, we only need to understand how to resolve it on the inboard side, where the nonaxisymmetric corrugations are present. To do this, we take a closer look at the magnetic field strength on the outermost flux surface of the Henneberg-Plunk device (Figure 1), where quasisymmetry is the worst⁶. Note that outside of the dashed lines, the contours of field strength can be approximated by straight horizontal lines, like in a tokamak. On the other hand, inside the dashed lines, the helical nature of the inboard side manifests via the helically slanted closed contours. This is where the quasisymmetry breaks, as point maxima of magnetic field strength, such as those at the centers of these closed contours, cannot exist in a perfectly quasisymmetric device⁸. However, in between the dashed lines, the field strength ranges only from 1.75 T to 2 T, or about 0.24 of the total range seen in the figure. Thus, assuming $\varepsilon \sim 0.2$, quasisymmetry can still be satisfied at the lowest order by approximating the field strength in between the dotted lines as constant. Assuming that everything outside of the dotted lines is in the axisymmetric region and that χ satisfies certain conditions, which we will derive shortly, the overconstraining problem is resolved. As a sidenote, a similar idea of having patches of constant $|\vec{B}|$ on a flux surface was considered in Ref 21, where Velasco et al introduce the concept of a piecewise omnigenous stellarator. Such a field with constant strength can be considered as approximately locally isodynamic²². Although exact globally isodynamic configurations can only be axisymmetric or helically symmetric^{23,24}, local approximate isodynamic constraints can be nonaxisymmetric²².

Proceeding under the assumption that in the non-axisymmetric region $\partial\Psi/\partial C_2 = O(\varepsilon^2)$ (i.e. Ψ only depends on $C_1 = B_v$ at the leading order), setting $a = 0$ and using expression (13), the Grad-Shafranov equation (12) in this region

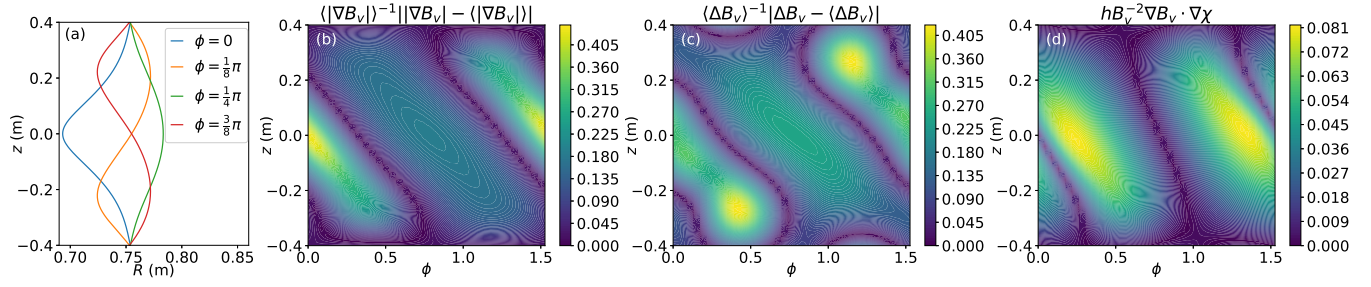


FIG. 2. The cross sections of the $B_v = 1.465$ T surface are shown at various values of ϕ in (a). In (b), the relative deviation of $|\nabla B_v|$ from its average value on the $B_v = 1.465$ T surface, $\langle |\nabla B_v| \rangle$; the same is shown for ΔB_v in (c). Finally, (d) shows that the normalized value of $g^{B_v, \chi} = \nabla B_v \cdot \nabla \chi$ is small. The quantities in panels (b), (c), and (d) are all shown on the $B_v = 1.465$ T surface, where these quantities are the highest.

becomes

$$\frac{g^{B_v, B_v}}{B_v^2} \frac{\partial}{\partial B_v} \left(B_v^2 \frac{\partial \Psi}{\partial B_v} \right) + \Delta B_v \frac{\partial \Psi}{\partial B_v} = -\frac{\mu_0}{B_v^2} \frac{dp}{d\Psi} - H(\Psi). \quad (14)$$

The RHS will be a function of only B_v , thus the LHS must be as well. The most straightforward way of achieving this is to demand that $g^{B_v, B_v} \equiv |\nabla B_v|^2 = f_1(B_v) + O(\varepsilon)$ and $\Delta B_v = f_2(B_v) + O(\varepsilon)$, where f_1 and f_2 are arbitrary functions. In addition, we show that $I = O(\varepsilon^2)$, which allows us to drop the $\Delta^* I$ term in equation (14), is obtained without us needing to impose a stringent constraint on it (Figure 2 d). Instead, we just impose a penalty on values of $g^{B_v, \chi}$ above a certain threshold to prevent the optimization from drifting towards large values of I . However, the $g^{B_v, \chi}$ in the final result is significantly below the threshold. Note that all of the constraints stated above only affect the vacuum scalar potential χ . Thus, once we find a vacuum magnetic field that satisfies these constraints to a sufficient degree, we can proceed to solve the Grad-Shafranov equations in the nonaxisymmetric and axisymmetric regions using standard methods.

To find an appropriate vacuum scalar potential, we must first choose a basis in the space of solutions to the Laplace equation, in which we will look for the scalar potential. We will choose our basis to be the following subset of cylindrical harmonics²⁵

$$\begin{aligned} \chi &= F_0 \phi + \chi_b, \\ \chi_b &= \sum_{n=1}^N \int_0^{k_{\max}} K_n(kR) (A_n(k) \cos kz \cos n\mathcal{N}\phi \\ &\quad + B_n(k) \cos kz \sin n\mathcal{N}\phi + C_n(k) \sin kz \cos n\mathcal{N}\phi \\ &\quad + D_n(k) \sin kz \sin n\mathcal{N}\phi) dk, \end{aligned}$$

where \mathcal{N} is the number of field periods. Here, we chose to have the R -dependence be via the modified Bessel function of the second kind K_n , rather than the ordinary Bessel functions J_n and N_n because the "banana coils" of the Henneberg-Plunk device are roughly helical. The magnetic field generated by a helical wire can be shown to depend on R via modified Bessel functions²⁶. We also excluded the modified Bessel function of the first kind I_n from the basis, as it goes to infinity as $R \rightarrow \infty$, whereas we need the field to decay to zero far from the banana coils. Finally, we introduce an additional

constraint on the basis, namely that $\partial \chi_b / \partial \phi|_{z=\pm h} = 0$, where h is a constant. The purpose of this constraint is to ensure that there are two $z = \text{const}$ planes where the value of B_v is roughly independent of ϕ , so that the nonaxisymmetric, B_v -dependent part of a flux surface can connect to the axisymmetric part in a small region where $z = \pm h + O(\varepsilon)$. Note that, since $B_v^2 = (\partial \chi / \partial R)^2 + (\partial \chi / \partial z)^2 + R^{-2} (\partial \chi / \partial \phi)^2$, there can still be a ϕ -dependence in B_v via $\partial \chi / \partial z$, which does not have to be independent of ϕ at $z = \pm h$ even if $\partial \chi_b / \partial \phi$ is zero, however, in practice this ϕ -dependence is negligible (Figure 2 a). After imposing this condition, the eigenvalue k , which could previously be continuous, can now only take a discrete set of values. After also imposing stellarator symmetry ($\chi(R, -z, -\phi) = -\chi(R, z, \phi)$), we obtain the basis that we will use:

$$\begin{aligned} \chi_b &= \sum_{n=1}^N \sum_{m=0}^M \left[b_{nm} K_n \left(\frac{2m+1}{2h} \pi R \right) \cos \left(\frac{2m+1}{2h} \pi z \right) \sin n\mathcal{N}\phi \right. \\ &\quad \left. + c_{nm} K_n \left(\frac{m+1}{h} \pi R \right) \sin \left(\frac{m+1}{h} \pi z \right) \cos n\mathcal{N}\phi \right]. \end{aligned} \quad (15)$$

Having decided on a basis, the series is truncated at $N = 1$ and $M = 2$, and initial guesses for the parameters F_0 , b_{nm} and c_{nm} are determined by performing a least squares fit of $\nabla \chi$ with $h = 0.4$ m to the vacuum magnetic field of the Henneberg-Plunk device, as calculated by a Biot-Savart code from the banana coil data. More specifically, we minimize the value of the integral $\int_{\mathcal{V}} |\nabla \chi - \vec{B}_{BS}|^2 dV$, where \mathcal{V} is defined as the subvolume of $0.55 \text{ m} \leq R \leq 1.8 \text{ m}$, $-0.8 \text{ m} \leq z \leq 0.8 \text{ m}$ where $|\vec{B}_{BS}|^{-1} h |\nabla \cdot \vec{B}_{BS}| \leq 0.05$, i.e. where the nonphysical divergence in the Biot-Savart field resulting from numerical error is sufficiently small. As this is a linear problem where the unknowns are a set of scalars, the linear algebraic equations for F_0 , b_{nm} , and c_{nm} are trivial to derive and solve.

In the next step, we try to minimize the dependence of g^{B_v, B_v} and ΔB_v on variables other than B_v by varying b_{nm} and c_{nm} while holding F_0 fixed. We seek to minimize the following objective with a least-squares approach, using the Trust Region

Dogleg approach²⁷, as implemented in the SciPy library²⁸:

$$\begin{aligned}
& \left[\max_{\vec{r} \in \mathcal{W}} h^2 \frac{|(\nabla B_v \times \nabla \chi) \cdot \nabla |\nabla B_v||}{B_v |\nabla B_v \times \nabla \chi|} \right]^2 \\
& + \left[\max_{\vec{r} \in \mathcal{W}} h^3 \frac{|(\nabla B_v \times \nabla \chi) \cdot \nabla \Delta B_v|}{B_v |\nabla B_v \times \nabla \chi|} \right]^2 \\
& + \left[R \left(\max_{\vec{r} \in \mathcal{W}} h \frac{|\nabla \chi \cdot \nabla B_v|}{B_v^2} - 4 \right) \right]^2.
\end{aligned} \quad (16)$$

Here, $R(x) = \max\{0, x\}$ is the ramp function and \mathcal{W} is defined as the subvolume of $0.53 \text{ m} \leq R \leq 1 \text{ m}$, $-0.4 \text{ m} \leq z \leq 0.4 \text{ m}$ where $B_v \leq 1.4 \text{ T}$. This optimization was lightweight enough to be done on a laptop, with the JAX automatic differentiation framework²⁹ being used to calculate the derivatives in (16). As shown in Figure 2, the resulting $|\nabla B_v|$ and ΔB_v both have a maximum deviation of $\sim 0.4 \sim 2\epsilon$ from their respective average values on a $B_v = \text{const}$ surface in the region of interest, which is defined as all points between $z = -0.4 \text{ m}$ and $z = 0.4 \text{ m}$ where $B_v \leq 1.465 \text{ T}$. The average values of $|\nabla B_v|$ and ΔB_v , to be used as coefficients in equation (14), are shown in Figure 3. The outermost flux surface will follow the $B_v = 1.465 \text{ T}$ surface in the nonaxisymmetric region. In addition, $h B_v^{-2} \nabla \chi \cdot \nabla B_v \leq 0.08 \sim 2\epsilon^2$, meaning that $I = O(\epsilon^2)$ and can be dropped from equation (12).

As discussed above, The last component in (16) is added to prevent the optimization from drifting towards large values of I by penalizing values of the normalized $g^{B_v \chi}$ above 4. However, the final $g^{B_v \chi}$ is far below the threshold. The final set of vacuum field coefficients that we will work with is given in Table I.

TABLE I. The set of vacuum field coefficients (in units of T · m) obtained by optimization.

F_0	-1.1031067415616023	c_{10}	1.7606108849811601
b_{10}	0.035820217604140225	c_{11}	-75.55668715202704
b_{11}	15.797529271426379	c_{12}	6833.099190151348
b_{12}	-341.8770726097677		

We now proceed to solve the Grad-Shafranov equation numerically, with $p(\Psi) = p_1 \Psi$ and $H(\Psi) = H_0 + H_1 \Psi$, where $p_1 = 10^7 / (4\pi) \text{ Pa/m}$, $H_0 = 0$ and $H_1 = 10 \text{ m}^{-1}$. We first consider the nonaxisymmetric region, where the Grad-Shafranov equation reduces to the ODE (14). This equation is solved on

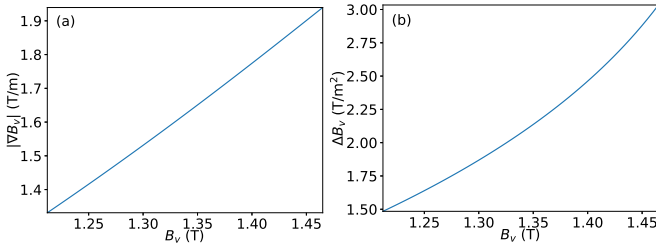


FIG. 3. The quantities $|\nabla B_v|$ (a) and ΔB_v (b), averaged on each $B_v = \text{const}$ surface.

the interval $B_v \in [1.212 \text{ T}, 1.465 \text{ T}]$, where the outermost flux surface is at $B_v = 1.465 \text{ T}$. Due to the fact that χ decays exponentially with R , $B_v = \text{const}$ surfaces approach $R = \text{const}$ surfaces as R increases. On the $B_v = 1.465 \text{ T}$ surface, the point at $z = 0$ moves 9.2 cm as ϕ changes from 0 to $\pi/4$ (Figure 2 a), whereas at $B_v = 1.212 \text{ T}$ the same point only moves by 3.05 cm or $\sim 2\epsilon^2$ of the minor radius. We will neglect this variation and try to patch the axisymmetric and nonaxisymmetric regions at $R = 0.91 \text{ m}$, which is the approximate location of the $B_v = 1.212 \text{ T}$ surface, making it the boundary between the two regions.

We impose a boundary condition of $\Psi = 0$. In addition, when solving the ODE (14), we have one more degree of freedom (either the value of Ψ at $B_v = 1.212 \text{ T}$ or its derivative at either endpoint) that needs to be fixed in order to have a unique solution. We choose $\partial \Psi / \partial B_v = -0.14 \text{ m/T}$ at $B_v = 1.465 \text{ T}$ as an initial guess. We will refine the solution iteratively in tandem with the solution in the axisymmetric region in a way that minimizes the surface current on the boundary between the two regions. The initial solution is then found using the Runge-Kutta 5(4) method³⁰.

In the axisymmetric region, the Grad-Shafranov equation (12) reduces to the familiar tokamak Grad-Shafranov equation

$$\Delta^* \Psi = - \frac{\mu_0 R^2}{F_0^2} \frac{dp}{d\Psi} - H(\Psi), \quad (17)$$

with the only difference being that the poloidal flux used in the standard form of the Grad-Shafranov equation has been replaced with the flux function Ψ . To solve this PDE, we will use a custom-made finite element solver. The domain on which we look for a solution is bounded by a superellipse given by the equation

$$\frac{(R - 1.015 \text{ m})^4}{(0.3065 \text{ m})^4} + \frac{z^4}{(0.48 \text{ m})^4} = 1,$$

with the section $\{(R, z) : R < 0.91 \text{ m}, |z| < 0.4 \text{ m}\} \setminus \{(R, z) : R > 0.87 \text{ m}, |z| > 0.36 \text{ m}, (R - 0.87 \text{ m})^2 + (|z| - 0.36 \text{ m})^2 >$

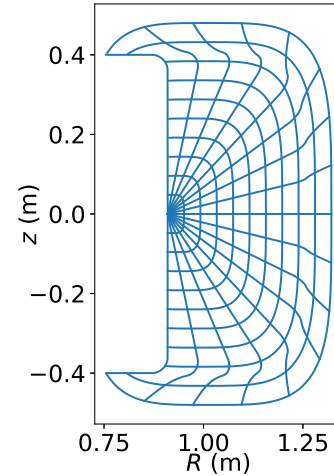


FIG. 4. The finite element grid that was used to solve equation (17). The resolution is reduced for clarity.

(0.04 m)² removed. The second set being subtracted accounts for the corners, which would otherwise have been at $R = 0.91$ m, $z = \pm 0.4$ m, being filleted with a radius of 0.04 m to avoid coordinate singularities. The resulting FEM grid is shown in Figure 4, with resolution reduced for clarity; the actual resolution was 50 radially and 32 poloidally. Dirichlet boundary conditions are imposed, with $\Psi = 0$ on the external boundary and Ψ being matched to the nonaxisymmetric solution on the internal boundary. The axisymmetric solution is then found using the Bubnov-Galerkin method; the basis functions are cubic Bezier splines with G^1 continuity at element edges. Finally, the average value of the derivative $\partial\Psi/\partial B_v$ on the line segment $R = 0.91$ m, $|z| < 0.36$ m (i.e., the part of the boundary between the axisymmetric and nonaxisymmetric regions that is between the two filleted corners) is calculated. The solution of (14) is then recalculated using the SciPy²⁸ implementation of a fourth-order collocation method discussed in Ref 31, with this value as a boundary condition for $\partial\Psi/\partial B_v$ at $B_v = 1.212$ T, while maintaining the boundary condition of $\Psi = 0$ at $B_v = 1.465$ T. This new nonaxisymmetric solution is then used to update the boundary conditions for the axisymmetric solution on the internal boundary, followed by recalculating the axisymmetric solution. This process is repeated until the value of $\partial\Psi/\partial B_v$ at $B_v = 1.212$ T converges to within 1%. Note that while this procedure minimizes the surface current on the internal boundary, it does not completely eliminate it, as the $\partial\Psi/\partial B_v$ on the axisymmetric side can vary with z , and the corresponding derivative on the nonaxisymmetric side is only matched to its average value, while local discontinuities still remain.

The flux surfaces of the resulting solution are shown in Figure 5. Some of the flux surfaces have sharp corners, which is an artifact of the imposition of a sharp boundary between the axisymmetric and nonaxisymmetric regions. In reality, a boundary layer would form between the two regions, smoothing the corners and alleviating the surface current issue discussed above. However, we will not attempt to find the boundary later correction to the solution shown in Figure 5, and instead will just use it as an initial guess for a stellarator opti-

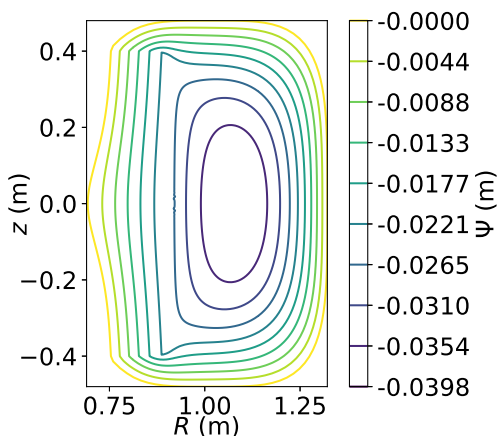


FIG. 5. The flux surfaces of the resulting approximate solution on the $\phi = 0$ plane, color coded by the value of Ψ on each surface.

mization, which we will present in the next section.

IV. REFINEMENT VIA CONVENTIONAL STELLARATOR OPTIMIZATION

In terms of quasisymmetry, the solution presented in the previous section has a quasisymmetry error that is several times higher than the configuration of Henneberg-Plunk⁶. Here, the error on a flux surface s is defined as

$$\sqrt{\sum_{\substack{m \\ n \neq 0}} \widehat{B}_{n,m}(s)^2 / \widehat{B}_{0,0}(s)^2}$$

where $\widehat{B}_{n,m}(s)$ are the Fourier modes of $|\vec{B}|$ on the flux surface.

However, by using the solution as the initial condition in a conventional stellarator optimization, we are able to bring the average value of the error, as defined above, down to 0.0158, which is comparable to Henneberg-Plunk (average error 0.0104).

Specifically, we truncate the Fourier representation of the initial condition to $n = 0, N, 2N$ toroidally and $m = 0, 1, \dots, 9$ poloidally, where $N = 4$ is the number of field periods, and represent the enclosed current $I(s)$ as a cubic spline sampled at 12 points, to reduce the number of degrees of freedom. We then minimize the following objective:

$$\sum_{m,n \neq 0} \frac{b_{mn}(s=1)^2}{b_{00}(s=1)^2} + 50 \max_i I(s_i)^2 + (t - t_*)^2, \quad (18)$$

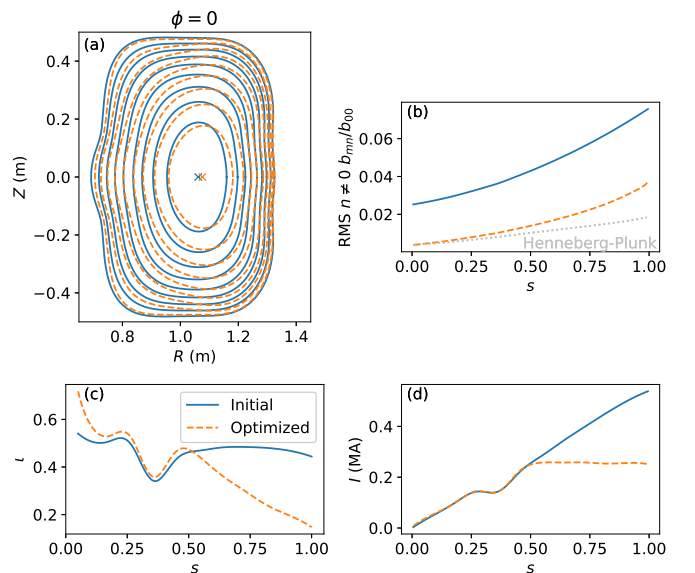


FIG. 6. Comparison of (a) boundary shape of the initial and optimized configuration and (b) quasisymmetry error. Also shown are the (c) ι and (d) enclosed current I . The initial configuration is obtained by passing the boundary and current from the solution in section III to VMEC. Both the initial and optimized configurations are calculated with a toroidal resolution of $n = 0, N, 2N$ and a poloidal resolution of $m = 0, 1, \dots, 9$.

where the first term represents the symmetry-breaking part of the Boozer spectrum at the boundary, the second term minimizes the total toroidal current inside equispaced discrete radii $s_i = i/(N-1), i = 0, \dots, N-1$, with $I(s_i)$ being the enclosed current in megaamperes, and the third term keeps the mean value of the rotational transform t close to t_* , which we take to be the mean t of the initial condition. Note that there is nothing in the minimization objective (18) that forces the configuration to be compact or tokamak-like: these features are purely a result of starting the optimization from a suitable initial condition.

A comparison of the initial and optimized configurations is shown in Figure 6. In the rotational transform plot, figure 6 c, the first five points from the axis were discarded, as VMEC is known to be inaccurate at the axis, due to a coordinate singularity³².

V. CONCLUSION

We have derived an asymptotic model that is valid for compact quasisymmetric stellarators with $\beta = O(\epsilon^2)$, under the assumption that the vacuum magnetic field is dominant ($\epsilon \ll 1$). However, non-vacuum effects can still contribute ($\nabla\chi \cdot \nabla = O(\epsilon)$). Just like in the large aspect ratio high- β model that we studied in Ref 19, the $O(\epsilon)$ correction to the magnetic field is overconstrained, being governed by both a Grad-Shafranov equation and the requirement that flux surfaces exist ($\vec{B} \cdot \nabla\Psi = 0$). This model is significantly more complicated than that of Ref 19, and as such, it does not seem to admit purely analytic solutions, except for trivial situations, such as axisymmetry or the large aspect ratio limit. Nevertheless, it enables us to disentangle the overconstraining problem in hybrid quasiaxisymmetric devices, similar to that studied by Henneberg and Plunk in Ref 6, by treating the problem in a piecewise manner, considering the axisymmetric and non-axisymmetric regions separately. We then apply standard numerical methods to solve the equations of our model in the two regions. Finally, we use this solution as an initial guess for a stellarator optimization using SIMSOPT.

In this paper, we have only considered one particular class of compact stellarators, namely, hybrid quasiaxisymmetric devices that have a purely axisymmetric region, and which allow Ψ to be approximated as a function of just B_v in the non-axisymmetric region. However, there are many more compact quasisymmetric stellarators that do not fit this mold, with NCSX being one prominent example. In the future, we intend to implement a numerical solver for the general problem, which will look for a solution in the space of functions of C_1, C_2 that minimizes the error in the Grad-Shafranov equation (12).

AUTHOR DECLARATIONS

The authors have no conflicts of interest to disclose.

ACKNOWLEDGMENTS

The authors thank Sophia Henneberg and Gabriel Plunk for providing the VMEC equilibria and vacuum field data for the device that they presented in Ref 6, and for fruitful discussions. The authors also thank Per Helander, Elizabeth Paul and Rogerio Jorge for fruitful discussions.

This research was supported by a grant from the Simons Foundation/SFARI (560651, AB) and the Department of Energy Award No. DE-SC0024548. Some computations were performed on the HPC system Viper at the Max Planck Computing and Data Facility (MPCDF).

DATA AVAILABILITY STATEMENT

The data that support the findings of this study are available from the corresponding author upon reasonable request.

- ¹A. Sykes, A. Costley, C. Windsor, O. Asunta, G. Brittles, P. Buxton, V. Chuyanov, J. Connor, M. Gryaznevich, B. Huang, J. Hugill, A. Kukushkin, D. Kingham, A. Langtry, S. McNamara, J. Morgan, P. Noonan, J. Ross, V. Shevchenko, R. Slade, and G. Smith, *Nuclear Fusion* **58**, 016039 (2017).
- ²A. W. Morris, *IEEE Transactions on Plasma Science* **40**, 682 (2012).
- ³S. Kaye, D. Battaglia, D. Baver, E. Belova, J. Berkery, V. Duarte, N. Ferraro, E. Fredrickson, N. Gorelenkov, W. Guttenfelder, G. Hao, W. Heidbrink, O. Izacard, D. Kim, I. Krebs, R. L. Haye, J. Lestz, D. Liu, L. Morton, J. Myra, D. Pfefferle, M. Podesta, Y. Ren, J. Riquezes, S. Sabbagh, M. Schneller, F. Scotti, V. Soukhanovskii, S. Zweben, J. Ahn, J. Allain, R. Barchfeld, F. Bedoya, R. Bell, N. Bertelli, A. Bhattacharjee, M. Boyer, D. Brennan, G. Canal, J. Canik, N. Crocker, D. Darrow, L. Delgado-Aparicio, A. Diallo, C. Domier, F. Ebrahimi, T. Evans, R. Fonck, H. Frerichs, K. Gan, S. Gerhardt, T. Gray, T. Jarboe, S. Jardin, M. Jaworski, R. Kaita, B. Koel, E. Kolemen, D. Kriete, S. Kubota, B. LeBlanc, F. Levinton, N. Luhmann, R. Lunsford, R. Maingi, R. Maqueda, J. Menard, D. Mueller, C. Myers, M. Ono, J.-K. Park, R. Perkins, F. Poli, R. Raman, M. Reinke, T. Rhodes, C. Rowley, D. Russell, E. Schuster, O. Schmitz, Y. Sechrest, C. Skinner, D. Smith, T. Stotzfus-Dueck, B. Stratton, G. Taylor, K. Tritz, W. Wang, Z. Wang, I. Waters, and B. Wirth, *Nuclear Fusion* **59**, 112007 (2019).
- ⁴H. Anand, O. Bardsley, D. Humphreys, M. Lennholm, A. Welander, Z. Xing, J. Barr, M. Walker, J. Mitchell, and H. Meyer, *Fusion Engineering and Design* **194**, 113724 (2023).
- ⁵M. C. Zarnstorff, L. A. Berry, A. Brooks, E. Fredrickson, G.-Y. Fu, S. Hirshman, S. Hudson, L.-P. Ku, E. Lazarus, D. Mikkelsen, D. Monticello, G. H. Neilson, N. Pomphrey, A. Reiman, D. Spong, D. Strickler, A. Boozer, W. A. Cooper, R. Goldston, R. Hatcher, M. Isaev, C. Kessel, J. Lewandowski, J. F. Lyon, P. Merkel, H. Mynick, B. E. Neilson, C. Nuehrenberg, M. Redi, W. Reiersen, P. Rutherford, R. Sanchez, J. Schmidt, and R. B. White, *Plasma Physics and Controlled Fusion* **43**, A237 (2001).
- ⁶S. A. Henneberg and G. G. Plunk, *Phys. Rev. Res.* **6**, L022052 (2024).
- ⁷P. E. Moroz, *Plasma Physics and Controlled Fusion* **40**, 1127 (1998).
- ⁸P. Helander, *Reports on Progress in Physics* **77**, 087001 (2014).
- ⁹A. H. Boozer, *Physics of Plasmas* **5**, 1647 (1998).
- ¹⁰A. Bader, M. Drevlak, D. T. Anderson, B. J. Faber, C. C. Hegna, K. M. Likin, J. C. Schmitt, and J. N. Talmadge, *Journal of Plasma Physics* **85**, 905850508 (2019).
- ¹¹D. A. Garren and A. H. Boozer, *Physics of Fluids B: Plasma Physics* **3**, 2822 (1991).
- ¹²D. A. Garren and A. H. Boozer, *Physics of Fluids B: Plasma Physics* **3**, 2805 (1991).
- ¹³M. Landreman and W. Sengupta, *Journal of Plasma Physics* **84**, 905840616 (2018).
- ¹⁴R. Jorge, W. Sengupta, and M. Landreman, *Nuclear Fusion* **60**, 076021 (2020).

- ¹⁵M. Landreman, *Journal of Plasma Physics* **88**, 905880616 (2022).
- ¹⁶E. Rodriguez, *Quasisymmetry*, Ph.D. thesis, Princeton University (2022), Available at <http://arks.princeton.edu/ark:/88435/dsp01x633f4257>.
- ¹⁷The model consists of two equations for the flux surface label: a GSE, which is a second-order elliptic PDE involving pressure and current, and a flux surface existence condition.
- ¹⁸W. Sengupta, N. Nikulsin, R. Gaur, and A. Bhattacharjee, *Journal of Plasma Physics* **90**, 905900209 (2024).
- ¹⁹N. Nikulsin, W. Sengupta, R. Jorge, and A. Bhattacharjee, *Journal of Plasma Physics* **90**, 905900608 (2024).
- ²⁰J. W. Burby, N. Kallinikos, and R. S. MacKay, *Journal of Mathematical Physics* **61**, 093503 (2020).
- ²¹J. L. Velasco, I. Calvo, F. J. Escoto, E. Sánchez, H. Thienpondt, and F. I. Parra, *Phys. Rev. Lett.* **133**, 185101 (2024).
- ²²W. Sengupta, E. J. Paul, H. Weitzner, and A. Bhattacharjee, *Journal of Plasma Physics* **87**, 905870205 (2021).
- ²³D. Palumbo, *Il Nuovo Cimento B (1965-1970)* **53**, 507 (1968).
- ²⁴W. K. Schief, *Journal of Plasma Physics* **69**, 465–484 (2003).
- ²⁵P. Morse and H. Feschbach, *Methods of Theoretical Physics*, Vol. 2 (McGraw-Hill, 1953).
- ²⁶T. Tominaka, M. Okamura, and T. Katayama, *Nuclear Instruments and Methods in Physics Research Section A: Accelerators, Spectrometers, Detectors and Associated Equipment* **459**, 398 (2001).
- ²⁷C. Voglis and I. Lagaris, in *WSEAS International Conference on Applied Mathematics*, Vol. 7 (2004).
- ²⁸P. Virtanen, R. Gommers, T. E. Oliphant, M. Haberland, T. Reddy, D. Cournapeau, E. Burovski, P. Peterson, W. Weckesser, J. Bright, S. J. van der Walt, M. Brett, J. Wilson, K. J. Millman, N. Mayorov, A. R. J. Nelson, E. Jones, R. Kern, E. Larson, C. J. Carey, Í. Polat, Y. Feng, E. W. Moore, J. VanderPlas, D. Laxalde, J. Perktold, R. Cimrman, I. Henriksen, E. A. Quintero, C. R. Harris, A. M. Archibald, A. H. Ribeiro, F. Pedregosa, P. van Mulbregt, and SciPy 1.0 Contributors, *Nature Methods* **17**, 261 (2020).
- ²⁹J. Bradbury, R. Frostig, P. Hawkins, M. J. Johnson, C. Leary, D. Maclaurin, G. Necula, A. Paszke, J. VanderPlas, S. Wanderman-Milne, and Q. Zhang, “JAX: composable transformations of Python+NumPy programs,” <http://github.com/google/jax> (2018), Software without accompanying journal publication.
- ³⁰J. Dormand and P. Prince, *Journal of Computational and Applied Mathematics* **6**, 19 (1980).
- ³¹J. Kierzenka and L. F. Shampine, *ACM Trans. Math. Softw.* **27**, 299–316 (2001).
- ³²D. Panici, R. Conlin, D. W. Dudt, K. Unalmis, and E. Kolemen, *Journal of Plasma Physics* **89**, 955890303 (2023).